DTU Library

Electronic structure, total energies, and STM images of clean and oxygen-covered Al(111)

Jacobsen, Joachim; Hammer, Bjørk; Jacobsen, Karsten Wedel; Nørskov, Jens Kehlet

Link back to DTU Orbit

Electronic structure, total energies, and STM images of clean and oxygen-covered Al(111)

J. Jacobsen, B. Hammer, K. W. Jacobsen, and J. K. Nørskov

Center for Atomic-scale Materials Physics and Physics Department,
Technical University of Denmark, DK 2800 Lyngby, Denmark

A set of density-functional calculations for clean and O-covered Al(111) are presented. At low O coverages the potential energy surface (PES) of chemisorbed O is investigated. The PES indicates large barriers (0.8 eV) against O diffusion and a large corrugation of the equilibrium O height over the Al(111) while only a moderate energy gain (5 eV per atom) is found upon O_2 dissociation over the surface. The possible existence of "hot" O adatoms after O_2 dissociation is discussed on the basis of the presented PES and existing dynamical simulations on model potentials. At high O coverages an attractive O-O interaction is identified together with an enhancement in the dipole moment induced per O atom. Finally, Tersoff-Hamann-type scanning tunneling microscopy (STM) topographs are derived based on the calculated one-electron wave functions and spectra. For the clean Al(111) a theoretical STM height corrugation compatible with the experimentally observed one is obtained if the tunneling conductance is assumed dominated by contributions from orbitals of atomic p character centered on the tip. For the O-covered Al(111) the theoretical topographs agree well with the observed ones.

I. INTRODUCTION

The interaction of oxygen with aluminum surfaces and, in particular, the Al(111) surface has been extensively studied in the past few decades. In 1976 Flodström et al.[1] found clear evidence in measured photoelectron spectra that an intermediate oxide phase or a chemisorbed oxygen state precedes the formation of the fully oxidized aluminum (Al_2O_3). Because O/Al(111) was thought to be a "prototype" simple chemisorption system, it was surprising that it turned out to be very difficult to characterize this initial chemisorption phase. Different experimental techniques gave contradictory results for the chemisorption site. The complexity of photoelectron spectra and electron energy loss spectra suggested the coexistence of several different chemisorption sites, and triggered by anomalously low measured changes in work function[2,3] the idea of a subsurface chemisorption site came up. The existence of this chemisorption site was also supported by theoretical work.[4] A critical review of the early literature is given by Batra and Kleinman in 1984.[5]

Now it seems commonly agreed that there is only a single chemisorption site. Oxygen sits in the threefold hollow fcc sites[6–10] 0.7 ± 0.1 Å above the first Al(111) layer[11–14,8] corresponding to an O-Al bond length of approximately 1.79 Å. This chemisorption site is also favored by several Hartree-Fock cluster calculations[15,16] and by the comparison of electronic band structure calculations [linearized augmented plane wave[17] (LAPW) and extended Hückel method[18]] with angular resolved photoemission spectra.[19,20] As first suggested by McConville et al.,[21] the different peaks in the photoelectron spectrum can be explained in terms of the different local environments arising when oxygen atoms gather together in small 1×1 islands, i.e., the coexistence of oxygen adatoms and oxygen in the interior and in the perimeter of an island.[7] This has also motivated the suggestion,[7] that the measured electron energy loss spectra[22–24] could be explained in the same way.

Recently, scanning tunneling microscopy measurements have focused attention on the O/Al(111) surface again.[9,10] One of the remarkable observations is that during the dissociation process, the oxygen atoms do not seem to settle in adjacent threefold sites on the surface, but rather form an even distribution over the whole surface. Given that there is no measurable oxygen diffusion at the temperature of the experiment, this points towards a transient ballistic motion of the oxygen atoms after dissociation.

An understanding of these scanning tunneling microscopy (STM) observations must involve an understanding of the potential energy surface (PES) on which oxygen moves on the Al(111) surface and the dynamics including the coupling between the oxygen motion and the Al phonons and electron-hole pair excitations. The only attempt, so far, is the work of Engdahl and Wahnström, which is based on an effective medium theory description of the interatomic interactions and molecular dynamics calculations of the dynamics.[25] The conclusion of this work is that the distribution of adsorbates after impact is mainly limited by randomization of the adsorbate motion, due to scattering from the corrugated potential seen by the oxygen atom, and the distance that the oxygen atoms can move after dissociation depends strongly on the kinetic energy available. An adsorption energy of 3.5 eV per atom does not give the observed randomlike distribution, which cannot be reproduced unless the atoms are given a kinetic energy of 9.5 eV per atom after dissociation.

In the present paper, we present a density functional calculation of the detailed potential energy surface of O outside the Al(111) surface. We calculate the equilibrium geometry, vibrational frequencies, the diffusion path and barriers, the chemisorption energy, adsorbate-adsorbate interactions, and the associated changes in the electronic structure. We compare these calculations with experimental observations where possible, and also discuss the STM adsorption experiments in the light of the results and the molecular dynamics calculations of Engdahl and Wahnström.[25] We find the fcc hollow site to be the stable chemisorption site, and we shall see that, as previously suggested, we can account for the measured electron energy loss spectra[22-24] from calculations of the vibrational frequencies of single oxygen adatoms and oxygen in the interior of a 1 × 1 oxygen island. We also calculate work functions in agreement with the early experimental measurements.[2,3] The comparisons of the theory with STM experiments require methods for generating STM images from the calculated electronic structure. We, therefore, present as an additional feature calculations of corrugations in the local density of states outside both clean and oxygen covered Al(111), which compare very well with experimental STM images for both systems.

The paper is organized as follows. First, we briefly describe the calculational method. Then we initiate the presentation of the results by first summarizing our results for the clean Al(111) surface. This section also includes a discussion of the corrugation of the STM images for the clean surface. In the following sections, we then show results for the PES for diffusion along the surface based on calculations with a quarter of a monolayer of chemisorbed oxygen, followed by a discussion of the oxygen-oxygen interactions at higher coverages. Before a more general discussion of the results with particular emphasis on the question of transient mobility after dissociation, we also present the calculations of the STM images expected for oxygen on Al(111). As we present the results of the calculation, we also discuss them in the light of available experimental results.

II. THE CALCULATIONAL METHOD

The calculations presented in this paper are all based on density-functional theory. The surface is modeled by a five or six layer repeated slab, with four "empty" layers between adjacent slabs. The one-electron wave functions are expanded in a plane wave basis with a kinetic energy up to 550 eV. 18 special k points are included in the entire first surface Brillouin zone corresponding to the (2×2) surface unit cell. For the Al atoms, we use the Bachelet-Hamann-Schlüter pseudopotential.[26] Since the O atoms have no p states in the core, we describe them by the Troullier-Martins pseudopotential[27] to make the plane wave expansion feasible. The one-electron Schrödinger equation is solved by means of alternating direct minimization steps[28] and subspace rotations.[29] The k summation is stabilized by employing for the occupation numbers a Fermi distribution with kT_e=0.1 eV.[29] Two

methods are used to treat exchange and correlation effects, the local density approximation (LDA) (Ref. 30) and the generalized gradient approximation (GGA).[31] The LDA calculations are performed self-consistently, whereas the nonlocal exchange-correlation corrections of the GGA are calculated from the LDA densities. All atomic relaxations are done according to the LDA functional.

Tests of the convergence in the cutoff energy and the number of k points show energy differences to be converged to within a few meV. Errors due to the finite thickness of the slab are an order of magnitude larger, when we calculate the interaction of oxygen atoms on the surface by comparing energies of systems having a different ratio of oxygen to aluminum atoms. We will return to this issue later.

III. CLEAN Al(111)

As a starting point, we consider the clean Al(111) surface. The lattice constant that minimizes the energy of bulk aluminum in the present total energy method is 3.96 Å. This value has been used in all calculations presented here. The distance between two bulk (111) layers is then 2.286 Å. In a clean Al(111) slab calculation with three layers fixed at bulk positions, and two layers allowed to relax freely, the equilibrium distance between the second and third layer is 2.242 Å and between the first and second layer is 2.309 Å. This corresponds to a relaxation of the second layer of −2%, and of the first layer +1%. The energy of this relaxation is 3.7 meV per surface atom. While the large second layer relaxation may be a finite size effect (insufficient number of slab layers or k points), we note that the finding of an outward first layer relaxation is in agreement with existing theoretical and experimental evidence. Experimentally, the relaxation of the first layer is found to be +0.9 ± 0.05 % (Ref. 32) and theoretically it has been reported to be +1.0 %.[33]

For the Al(111) surface, STM experiments have shown a very large corrugation of the constant current contours at least for small tip-metal distances. This has been quite a puzzle, since the Al(111) surface shows a very "flat" charge density and since surface states and other features that could give rise to a large corrugation do not exist in the appropriate energy range. Before discussing the STM images of O adsorbed on this surface we, therefore, first consider the clean surface in some detail.

We base our description of the tunneling rate between a surface and a tip on the Bardeen approximation and the treatment of Tersoff and Hamann.[34] In this treatment, the relevant electronic wave function at the tip is assumed to have a spherical symmetry around a center of curvature r_0. This assumption leads to the result that the tunneling conductance is proportional to the local density of states at the Fermi level, taken at r_0:

$$\sigma_s \propto \sum_{i,k} |\psi_{i,k}(r_0)|^2 \delta(E_{i,k} - E_f) \quad .$$

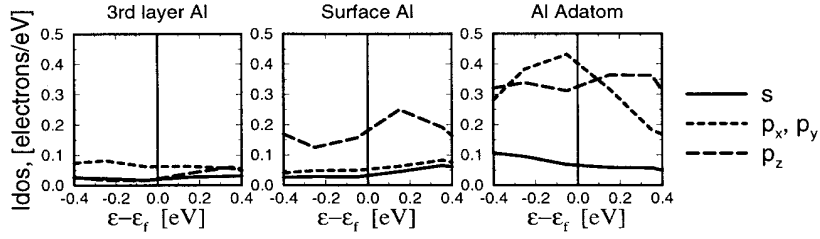A realization of this is the case where the relevant tip

FIG. 1. The density of states in the vicinity of the Fermi energy, projected on s and p orbitals positioned on aluminum atoms in the third layer (bulklike), in the surface layer, and as an adatom. The Fermi level is indicated by a vertical line.

state is an s state at the tip atom, i.e., the atom closest to the surface. This can be generalized to p or d tip states.[35] If, for example, the relevant tip state is a p_z state, one finds

$$\sigma_{p_z} \propto \sum_{i,k} \left| \frac{\partial \psi_{i,k}}{\partial z}(r_0) \right|^2 \delta(E_{i,k} - E_f) \quad .$$

Figure 1 shows the density of states in an energy window around the Fermi energy projected onto aluminum atomic orbitals placed in various aluminum sites. The local density of states of an aluminum adatom is predominantly of p character. Although the corrugation of the STM image of Al(111) was measured using a tungsten tip,[36] the atomic resolution was obtained upon a tip preparation, where the voltage was increased by a factor of 15 for a short time, resulting in a tip lengthening of 25 Å. A reasonable explanation of the tip lengthening is that aluminum is transferred to the tip. Therefore, it is possible that the local density of states on the tip atom is well described by that on an aluminum adatom. If this is the case, the STM tip will follow the contours of constant σ_{p_z} rather than those of constant σ_s.

Figure 2 shows for clean Al(111) the s- and p-type STM images calculated as the heights above the surface of constant σ_s and σ_{p_z}, respectively. The images are hardly distinguishable. The vertical corrugation is 0.15 Å in both cases, with the atop positions imaged higher than the hollow sites. However, the mean distance to the surface is different, the p-type STM being 0.8 Å further away. Figure 3 shows the vertical corrugation, Δz as a function of the mean distance to the surface, $\langle z \rangle$ in a log-linear plot for the two types of STM imaging. The zero point of the distance to the surface is an Al(111) inter-
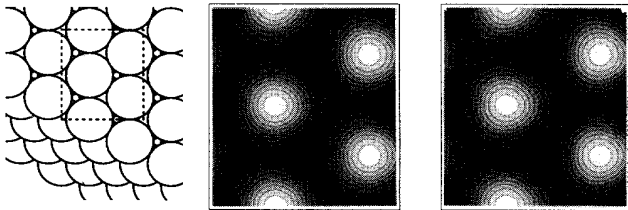
layer distance. To a good approximation the distance to the surface, when the tip atom is above atop positions, will be $\langle z \rangle + \Delta z/2$, and $\langle z \rangle - \Delta z/2$ when the tip atom is above hollow sites. Also shown in Fig. 3 is the experimentally observed corrugation of the STM image.[36] Here, the absolute value of the distance to the surface is unknown. Each of the three data sets can be well described by straight lines having similar slopes. The s-type STM image shows a maximum corrugation of less than 0.2 Å outside the surface in clear contrast to the experiment. The corrugation of the p-type STM images on the other hand shows a maximum corrugation before contact, which is just slightly smaller than the experimental values. Furthermore, it agrees with the *a priori* surprising observation that a measurable corrugation was found in a range of distances to the surface of 2 Å.[36]

The origin of this corrugation, we believe, is also to be found in Fig. 1. If we look at the graph showing the local density of states at a surface aluminum atom, we see that it has predominantly p_z character in the vicinity of the Fermi level. This p_z component is fairly large compared to the local density of states at the Fermi level at a bulk aluminum atom, and gives rise to the corrugation, because of its peak in magnitude in the direction normal to the surface from the aluminum sites in the surface layer.

IV. THE PES FOR O/Al(111) AT Θ =0.25

The PES for O on Al(111) is examined by putting an oxygen atom at different sites on the surface and mini-

FIG. 2. In the middle and to the right, respectively, the calculated contours of constant σ_s (s-type) and σ_{p_z} (p-type) outside a clean Al(111) surface schematically shown to the left. In both cases, the vertical corrugation is 0.15 Å. In the p-type STM the average height above the surface is $\langle z \rangle - z_0$=0.9 Å, whereas in the s-type STM $\langle z \rangle - z_0$=0.1 Å, z_0 being one Al(111) layer spacing outside the position of the surface layer.
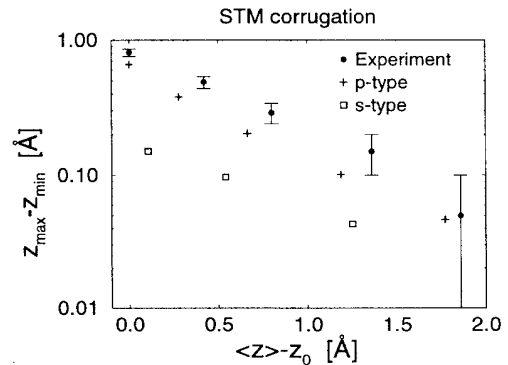

FIG. 3. The calculated corrugation of contours of constant σ_s and σ_{p_z} shown together with the corrugation of the measured STM images (Ref. 36) as a function of tip-sample distance. The zero point of the latter is one Al(111) layer spacing outside the position of the surface layer for the calculated corrugations, whereas it is unknown for the experimental points.

mizing the energy with respect to the height of oxygen above the surface. Subsurface sites are also examined. The surface unit cell is 2×2, and the slab has five layers. The calculations are first done with all Al atoms static, and afterwards with the two first layers allowed to relax.

The results within the LDA for a fixed Al lattice are summarized in Fig. 4. Here, we show the energy of an oxygen atom along the path shown in the inset from the fcc site over a bridge site into an hcp site and further over the atop site. The figure is constructed by first determining the energy in the high symmetry points (including minimization of the O height above the surface) followed by a calculation of the curvatures at these points. One small effect that comes out of this is that the maximum over the bridge site is not exactly halfway between the fcc and the hcp site. Rather, the transition state between the two local minima of the PES is found to be 57% of the way from the fcc site towards the hcp site.

The change in energy along the path shown is quite substantial. The fcc site is the preferred site in agreement with experimental findings,[6–10] and the barrier for diffusion to a neighboring hcp site is as large as 0.8 eV. The hcp site is 0.37 eV higher in energy than the fcc site. It is extremely unfavorable for oxygen to be positioned on top of an Al surface atom. The results are summarized in Table I. Here, we also show the effect of including Al lattice relaxations and of including the GGA correction as described above. Clearly neither of the two effects change the results significantly. When both the (LDA) relaxations and the GGA correction are included, the diffusion barrier decreases to 0.75 eV, which is still substantial, and which is in accordance with the experimental observation that adsorbed oxygen is not mobile at 300 K.

From the calculations, we also deduce the equilibrium height of the oxygen atom at various sites on the surface. The corrugation of this quantity is illustrated in Fig. 5. The height, z_0^{fcc} of 0.86 Å above the Al(111) layer, when O is in the fcc site, is slightly higher than the experimental value of 0.7 ±0.1 Å;[11–14,8] however, we shall see
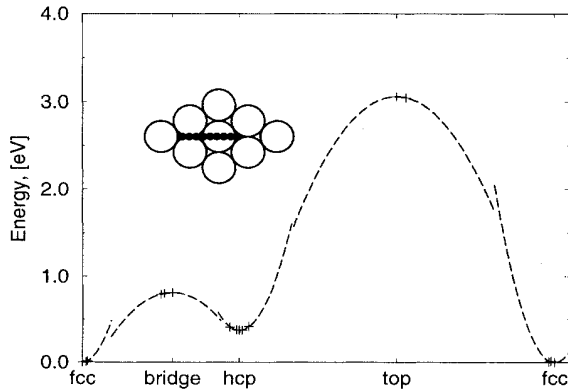

FIG. 4. The energy along the path shown in the inlet is estimated from the calculated LDA energies and energy curvatures for oxygen positioned in fcc, bridge, hcp, and top sites, respectively. The dashed lines are parabolas fitting the calculated points marked with plus signs.

TABLE I. The corrugation in the potential energy and vibrational frequency of 0.25 ML O chemisorbed on Al(111). Whenever included, the relaxations are done according to the LDA functional.

| O site | LDA unrelaxed | | | LDA relaxed | GGA relaxed |
	ΔE (eV)	$\nu_\perp$ (meV)	$\nu_\parallel$ (meV)	ΔE (eV)	ΔE (eV)
fcc	0	51	53	0	0
hcp	+0.37	53	47	+0.35	+0.37
bridge	+0.81	60		+0.79	+0.75
top	+3.06			+3.06	+2.94

how this improves when we treat the 1×1 oxygen overlayer. The maximum spatial corrugation is found to be $z_0^{top} - z_0^{fcc} = 0.78$ Å, whereas the maximum spatial corrugation along the diffusion path is $z_0^{bridge} - z_0^{fcc} = 0.18$ Å. The spatial corrugation of the O/Al system changes very little if two Al layers are allowed to relax.

In Table I, we also include the calculated vibrational frequencies. To get the vibrational frequencies, a small displacement (a few percent of an Å) of the oxygen position was made, and the total energy was calculated again. Some of the oxygen positions for which the total energy was calculated are marked in Fig. 4. If ΔE is the energy change when oxygen is displaced Δb then the vibrational quantum (loosely termed the frequency) is

$$\hbar\omega = h\nu = \hbar\sqrt{\frac{2\Delta E}{M_{\rm eff}\Delta b^2}} \ .$$

$M_{\rm eff}$ was assumed to be the mass of oxygen in all cases. This could give rise to a small underestimate of the frequencies. We estimate the perpendicular and the parallel frequency to be 51–53 meV. This agrees reasonably well with one of the modes observed experimentally [40–50 meV (Ref. 22) or 50–54 meV (Ref. 23)]. We shall return to the comparison with experiment later, when we treat a 1×1 O overlayer.

The most stable subsurface chemisorption site is found to be 0.68 Å above the second Al(111) layer in the octahedral position, and is 1.86 eV higher in energy compared to the fcc site above the surface. In this calculation two Al layers were allowed to relax, and the equilibrium bond length to the second layer Al atoms is 1.83 Å, those in the first layer being at a distance of 2.53 Å.
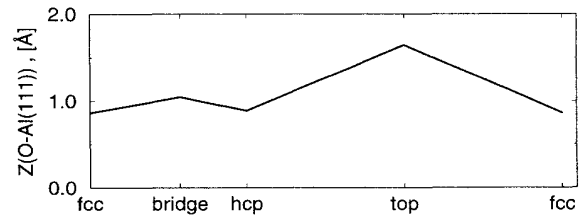

FIG. 5. The height of O above the top Al(111) layer. The two axes have the same scale. The O sites are the same as in Fig. 4.

V. ESTIMATE OF THE CHEMISORPTION ENERGY

We estimate the chemisorption energy per O_2 molecule in the following way. Using our nonspin-polarized pseudopotential code, we can calculate the energies of a single oxygen atom (E_O), a clean Al slab (E_{Al}), and the oxygen atom on the Al slab $(E_{O,Al})$, all calculations using exactly the same super cell to minimize numerical errors. Using the atomic code used to generate the oxygen pseudopotential, we find the energy cost of unpolarizing atomic oxygen to $E_{unpol}=1.409$ eV/atom. The atomization energy of O_2 has been calculated by Becke[37] to be $E_b=3.73$ eV/atom using LDA and $E_b=2.95$ eV/atom using PW-GGA. From these energies, we estimate the chemisorption energy per atom to be

$$E_{chem} = (E_O - E_{unpol} - E_b) + E_{Al} - E_{O,Al} \ .$$

The LDA and GGA results with and without Al relaxations are given in Table II. LDA overbinds the oxygen atoms to the aluminum surface; however, the LDA overbinding of the molecule is even stronger, and as a net result GGA gives the largest chemisorbtion energy of oxygen to the aluminum surface with respect to the oxygen molecule. Allowing Al to relax is of minor importance only increasing the chemisorption energy per atom by 0.08 eV. The resulting GGA chemisorption energy is 5.0 eV/atom.

VI. THE O-O INTERACTION ON Al(111)

In this section, the variation of the oxygen chemisorption energy with coverage is discussed. To do this, it is necessary to compare total energies of super cells having a different ratio of oxygen to aluminum atoms. Special care, therefore, has to be taken to monitor possible finite site effects.

One possible effect is the following. When oxygen absorbs on an aluminum surface electrons are transferred from the metal to orbitals on the oxygen atom, as can be seen from the next section. If the slab is made out of a finite number of Al atoms, this will lower the Fermi level, and the aluminum atoms will be slightly positively charged. Imagine another oxygen atom is brought to the same slab. There will now be an additional energy cost associated with removing electrons from the positively charged region. This finite size error will show up as a repulsive contribution to the interaction of the oxygen

TABLE II. The LDA and GGA result for the chemisorption energy per O atom, with and without Al relaxations. The chemisorption energy is given with respect to the energy level of molecular oxygen. The O coverage is 0.25 ML.

	Al unrelaxed	Al relaxed
LDA	4.69 eV	4.76 eV
GGA	4.92 eV	5.00 eV

atoms on the surface.

To estimate the importance of these finite size effects, the calculations with varying oxygen coverages are done for two different slab thicknesses, five and six Al layers. Also as a test, a calculation having a coverage of 0.25 ML on both slab sides was carried out. For sufficiently thick slabs this should give the same oxygen binding energy as obtained in the calculation having the same coverage on one side only. Figure 6 shows the geometry of systems treated.

Table III summarizes the LDA and GGA results for five and six Al layer slabs with the three different coverages shown in Fig. 6. Note that compared to the effect of changing the slab thickness, the inclusion of GGA has a very little effect. The important observation is that the oxygen energy is lowered (the binding energy increases) as the number of O-O nearest neighbor bonds is increased. This predicts island formation for coverages less than 1 ML, in agreement with experiment.[9,10] This conclusion is independent of the slab thickness or the presence of adsorbates on both sides of the slab, but the dependence of the binding energy on these factors points to the level of accuracy of the resulting bond energies.

The strong attraction between the oxygen atoms on Al(111) can also be seen in the density of states. Figure 7 shows the density of states projected onto the atomic p_x, p_y, and p_z states for low and high coverage. It can be seen that the p_z projection is rather unaffected by the coverage, whereas the (degenerate) p_x and p_y states are broadened considerably when there are oxygen nearest neighbors present. The total weight on the O $2p$ states increases at higher coverages, showing how the charge transfer increases to make the bond more ionic. This effect is evident when we look at the calculated O-induced dipole moments shown in Table IV. The dipole moments *increase* as the O coverage increases. This is again the opposite of the behavior observed for other metals. Usually, the two dipoles that are brought closer to each other will depolarize each other, resulting in a smaller dipole moment. For the O/Al(111) case, the O-O interactions win over the depolarization effects. The calculated oxygen induced change in work function at 0.25 ML coverage for the six layer slab is 0.09 eV, in good agreement with experiment.[2,3] At 1 ML, the work function shift becomes as much as 1 eV; however, this number is more strongly influenced by the finite slab thickness.

The attraction between the oxygen atoms on the Al(111) surface is in contrast to the strong repulsion that is usually found between adsorbed oxygen atoms on other
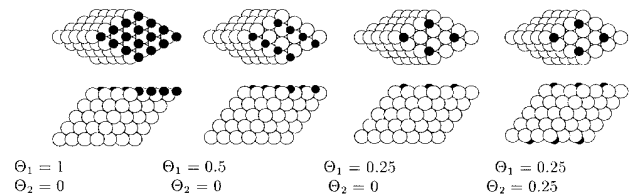

$\Theta_1 = 1$ $\Theta_1 = 0.5$ $\Theta_1 = 0.25$ $\Theta_1 = 0.25$
$\Theta_2 = 0$ $\Theta_2 = 0$ $\Theta_2 = 0$ $\Theta_2 = 0.25$

FIG. 6. The super cells repeated 2×2 times seen from above, and from the side. Θ_1 and Θ_2 are the oxygen coverages on the two sides in units of Al(111) monolayers.

TABLE III. The LDA and GGA result for the oxygen energy level in eV for different oxygen coverages (Θ_1 and Θ_2) on the two sides of the slab, having five or six Al layers, respectively. In each column 0.25 ML of oxygen on one side only defines the zero point of the energy.

		Five Al layers		Six Al layers	
Θ_1	Θ_2	LDA	GGA	LDA	GGA
1	0	-0.349	-0.365	-0.500	-0.517
0.5	0	-0.086	-0.089	-0.149	-0.152
0.25	0	0	0	0	0
0.25	0.25	0.079	0.081	-0.055	-0.054

TABLE IV. The net dipole moments per oxygen atom absorbed in different coverages on one side only of a slab of six Al layers. Also shown is the distance of the oxygen atoms to the first Al(111) layer, $z_{O,Al}$.

Θ	μ (eÅ)	$z_{O,Al}$ (Å)
1.0	-0.038	0.73
0.5	-0.025	0.82
0.25	-0.013	0.87

metal surfaces.[38,39] We suggest that the main reason for this is to be found in the fact that for Cu, Ni, and the other noble and transition metals mostly the s states are active in the bond formation. For aluminum the p states also contribute significantly and this opens new possibilities for hybridization, which again leads to stronger bonding configurations.

Returning now to the dependence on coverage of the interaction of oxygen with the Al(111) surface, we note that the stronger bond at higher coverage is reflected in a shorter bond length. In Table IV, we show that the oxygen atoms move in by 0.14 Å when the coverage reaches one monolayer. It can be seen that the shorter bond length of the $p(1 \times 1)$ overlayer is in better agreement with experiment than the bond length found for the $p(2 \times 2)$ overlayer. This is very reasonable, since the attractive interactions should give rise to island formation (as in the STM,[9,10] low-energy electron diffraction,[40,13,14] and angle-resolved photoemission spectroscopy[19,20] experiments) and experiment therefore primarily access the short bond length associated with the (1×1) structure.

Table V gives the frequencies of the vibration of oxygen adatoms perpendicular and parallel to the surface for 0.25 and 1 ML oxygen coverage. The vibrational frequencies of the more strongly bonded oxygen atoms sitting in (1×1) islands are increased by a little more than 20%. We believe this to be a lower bound for two
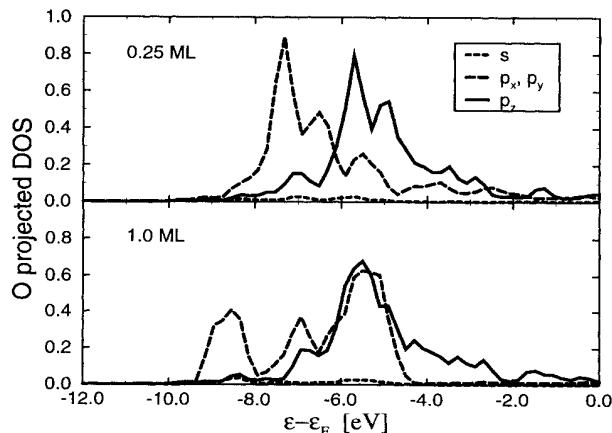
reasons. First, this calculation was done on a five layer aluminum slab, where the oxygen-oxygen attraction is underestimated, which gives reason to believe that the increase in vibrational frequency as the oxygen atoms are brought closer together, could also be underestimated. Second, we calculate the infinite wavelength frequency, and thereby do not include the dispersion due to the interaction. Experimentally three modes are observed at 40–54 meV, 65–81 meV, and 105–120 meV.[22–24] The high frequency mode is believed to originate from the oxide (Al_2O_3) phase.[22–24] The low frequency mode, which is weak or even absent,[24] fits extremely well with the calculated vibrational frequency of the oxygen adatom [the most recent observation of the peak is 50–54 meV (Ref. 23)]. The intermediate and stronger peak, we believe, originates from oxygen atoms in the interior of an island. We calculate this frequency to be 64–66 meV. The fact that the low frequency mode is weak agrees well with the oxygen island formation. The present understanding of the vibrational spectrum suggests that the appearance of the different peaks depends on the preparation of the surface. If, for example, an Al(111) surface is prepared on which only single oxygen adatoms exist, only the low frequency mode should be found. The vibrational frequencies of an oxygen atom in the perimeter of an island or in a dimer has not been calculated. If a significant fraction of the oxygen atoms adsorbed on the Al(111) surface occupies such positions, they may show up as additional peaks in the spectrum.

VII. STM IMAGING

In this section, we present the calculated STM images for oxygen adatoms and oxygen dimers on the Al(111) surface. The main reason for doing this is the following. The surprising conclusion that oxygen atoms travel a long distance apart upon dissociation is based on the radial distribution of the oxygen atoms as obtained from STM experiments.[9,10] Obviously, it is of crucial importance for the conclusion, that the appearance of oxygen adatoms

FIG. 7. The density of states projected on s and p atomic orbitals of an oxygen atom chemisorbed in a 2×2 structure (above) and in a 1×1 structure (below) on the Al(111) surface.

TABLE V. The normal and parallel vibrational frequencies of oxygen in a 1×1 (1 ML) and 2×2 (0.25 ML) structure on a five layer aluminium slab.

Θ	$\nu_\perp$ (meV)	$\nu_\parallel$ (meV)
1.0	64	66
0.25	51	53

and oxygen dimers, respectively, can be uniquely identified. However, the interpretation of STM images is not always straightforward. Thus, our aim is to calculate how the oxygen adatoms and oxygen dimers should appear in STM images, and we shall see how this provides justification for the interpretation of the experimental images.[9,10]

Figure 8 shows calculated STM images of an oxygen dimer and a single oxygen adatom on the Al(111) surface. Note that the calculational unit cells are larger than the ones discussed so far. The number of special k points included in the entire first surface Brillouin zone is 16 for the $3 \times \sqrt{3}$ unit cell and 6 for the 3×3 unit cell. The images are contours of constant σ_s. As was the case for the clean Al(111) the contours of constant σ_{p_z} look very similar, but are shifted further away from the surface. The oxygen atom appears as a dark spot with a brighter region in the center. The dimer appears as an elongated dark spot with a bright region on each of the individual oxygen atoms. This is exactly how oxygen is identified in the experiment,[9,10] verifying that indeed it is possible experimentally to see the oxygen atoms, and distinguish between single adatoms and dimers.

VIII. DISCUSSION

In the present paper, we have presented a detailed calculation of the potential energy surface for oxygen atomically adsorbed on Al(111). The main conclusions are as follows.
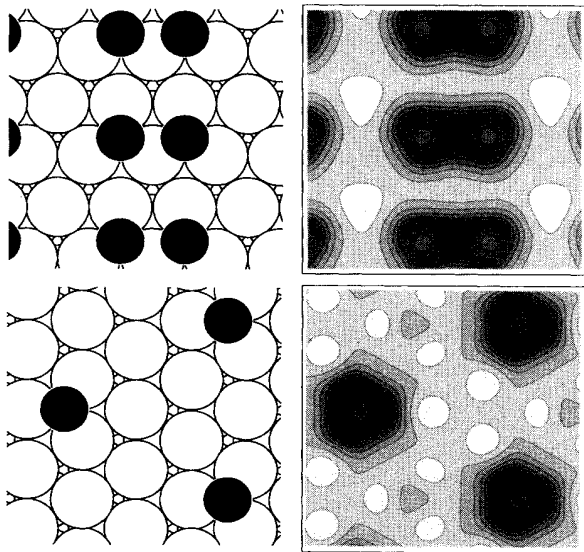

FIG. 8. Above: an oxygen dimer in a $3 \times \sqrt{3}$ unit cell. Below: an oxygen atom in a 3×3 unit cell. To the right calculated STM images are shown, and to the left the atomic positions, with the oxygen atoms small and dark, and the aluminum atoms white. In the STM images, the gray scale is after the height above the surface, in which a local density of states of 0.001 $e(\text{Å}^3\,\text{eV})$ is found. Black is 1.9 Å above the first Al(111) layer, and the spacing is 0.1 Å.

(1) The adsorption energy, vibrational frequencies, bond lengths, and dipole moments depend critically on the coverage. The lowest-energy state is found to be a full monolayer (1×1) structure with oxygen in the threefold fcc sites. The calculation supports the earlier suggestions[9,10] that oxygen tends to form islands and it is shown that the experimental observation of several different vibrational frequencies can be explained by assuming that at low temperatures single adsorbed oxygen atoms and oxygen islands coexist on the surface.

(2) The barrier for diffusion is large, 0.8 eV, and the potential energy surface quite corrugated, i.e., the lowest-energy state over the bridge and atop sites are considerably further away from the surface than in the equilibrium fcc site. This is in accordance with the experimental observation that diffusion is very slow at room temperature.[10]

(3) Simulations of the STM topographs of the clean Al(111) surface show a considerable corrugation at small tunneling distances, which is attributed to the p_z states of the surface, which dominate the density of states at the Fermi level. The variation of the STM corrugation of the surface with distance is found to be very similar to the experimentally observed variation.[36]

(4) Simulations of the STM topographs for oxygen covered Al(111) show the O atoms as a fairly large depression with a small peak in the middle, again in complete agreement with experimental observations.[10]

It can, therefore, be concluded that a fairly consistent picture of atomic oxygen chemisorption on Al(111) is developing.

The dynamics of the adsorption process is much less understood. In particular, the STM results that the oxygen atoms are quasirandomly distributed after low temperature deposition[10] are hard to understand in terms of a transient mobility of the oxygen atoms along the adiabatic potential energy surface. The reason is the following. As mentioned in the Introduction, Wahnström and Engdahl have carried out molecular dynamics simulations of the mobility of oxygen atoms that are given various amounts of kinetic energy along the surface.[25] The kinetic energy is supposed to come from the chemisorption energy, which is released during adsorption. They found that kinetic energies larger than 9 eV per atom are needed to give a quasirandom distribution. This is far larger than the 5 eV per atom that we find as the chemisorption energy (cf. Table II). The molecular dynamics simulations are based on an effective medium (EMT) potential, which has essentially the same spatial corrugation, but an energy corrugation smaller by a factor of two, compared to the potential we present here.[25] In particular, the barrier for diffusion in the EMT potential is 0.3–0.4 eV, depending on Al relaxations. Thus, with the present potential, an even larger initial kinetic energy of the oxygen atoms would be needed to get agreement with the experimentally observed radial distribution upon dissociation.

The most important parameter determining the mobility of the "hot" oxygen atoms along the surface is the rate at which the kinetic energy along the diffusion path is dissipated into other degrees of freedom. Accord-

ing to the simulations, this dissipation is dominated by transfer of the energy into the other oxygen degrees of freedom perpendicular to the diffusion path.[25] Collisions with corrugations in the potential very quickly randomizes the motion. Dissipation into the substrate degrees of freedom then takes place on a longer time scale. The randomization is determined by the spatial corrugation of the potential, which turns out to be exactly the same in the EMT potential and in our calculation (cf. Fig. 5). We, therefore, conclude that a simple picture of the oxygen atoms using the chemisorption energy to migrate over large distances over the surface on the adiabatic potential energy surface is in conflict with the simulations of Wahnström and Engdahl.

There are other interesting aspects of the oxygen adsorption process that may point to possibilities for explaining the STM results. It is well established that oxygen adsorption on Al surfaces is strongly nonadiabatic.[41] Oxygen adsorption gives rise to chemiluminescence as well as to exoelectron emission,[41] as has also been seen for other oxygen adsorption systems lately.[43] The nonadiabatic effects are believed to be related to the transfer of electrons from the metal states to the antibonding O_2 states. If this transfer does not take place instantaneously when the molecular levels cross the Fermi level, an electron-hole pair excitation results, which may decay via photon emission or an Auger process.

To get a large mobility along the surface, it is necessary for the oxygen atoms to move further away from the surface where the corrugation of the potential is small. Following the discussion of Hellberg et al.,[42] we suggest that one of the electron transfers into the antibonding O_2 levels results in the two O atoms being repelled strongly from each other. This transfer may take place at some distance from the surface, where the corrugation is small, and depending on the orientation[44] of the O_2 (or O_2^-) molecule when the electron transfer takes place, one of the atoms (or ions) may be "shot" out of the surface and follow a "cannonball"-like trajectory spending most of the time far from the surface, where the corrugation is very small. This picture is supported by the observation that in similar processes, O^- (Ref. 45) or other ionic parts (Refs. 46 and 42) of the adsorbing molecule has been observed.

ACKNOWLEDGMENTS

[1] S. A. Flodström, R. Z. Bachrach, R. S. Bauer, and S. B. M. Hagström, Phys. Rev. Lett. **37**, 1282 (1976).

[2] P. O. Gartland, Surf. Sci. **62**, 183 (1977).

[3] P. Hofman, W. Wyrobish, and A. M. Bradshaw, Surf. Sci. **80**, 344 (1979).

[4] D. M. Bylander and L. Kleinman, Phys. Rev. B **28**, 523 (1983).

[5] I. P. Batra and L. Kleinman, J. Electron Spectrosc. Relat. Phenom. **33**, 175 (1984).

[6] J. Wintterlin, H. Brune, H. Hoger, and R. J. Behm, Appl. Phys. A **47**, 99 (1988).

[7] P. S. Bagus, C. R. Brundle, F. Illas, F. Parmigiani, and G. Polzonetti, Phys. Rev. B **44**, 9025 (1991).

[8] M. Kerkar, D. Fischer, D. P. Woodruff, and B. Cowie, Surf. Sci. **271**, 45 (1992).

[9] H. Brune, J. Wintterlin, R. J. Behm, and G. Ertl, Phys. Rev. Lett. **68**, 624 (1992).

[10] H. Brune, J. Wintterlin, J. Trost, G. Ertl, J. Wiechers, and R. J. Behm, J. Chem. Phys. **99**, 2128 (1993).

[11] J. Stöhr, L. I. Johansson, S. Brennan, M. Hecht, and J. N. Miller, Phys. Rev. B **22**, 4052 (1980).

[12] D. Norman, S. Brennan, R. Jaeger, and J. Stöhr, Surf. Sci. **105**, L297 (1981).

[13] F. Soria, V. Martinez, M. C. Munoz, and J. L. Sacedon, Phys. Rev. B **24**, 6926 (1981).

[14] V. Martinez, F. Soria, M. C. Munoz, and J. L. Sacedon, Surf. Sci. **128**, 424 (1983).

[15] B. N. Cox and C. W. Bauschlicher, Surf. Sci. **115**, 15 (1982).

[16] R. Broer, I. P. Batra, and P. S. Bagus, Philos. Mag. B **51**, 243 (1985).

[17] D. Wang, A. J. Freeman, and H. Krakauer, Phys. Rev. B **24**, 3092 (1981).

[18] I. P. Batra and O. Bisi, Surf. Sci. **123**, 283 (1982).

[19] W. Eberhardt and F. J. Himpsel, Phys. Rev. Lett. **42**, 1375 (1979).

[20] P. Hofman, C. V. Muschwitz, K. Horn, K. Jacobi, A. M. Bradshaw, K. Kambe, and M. Scheffler, Surf. Sci. **89**, 327 (1979).

[21] C. F. McConville, D. L. Seymour, D. P. Woodruff, and S. Bao, Surf. Sci. **188**, 1 (1987).

[22] R. L. Strong, B. Firey, F. W. de Wette, and J. L. Erskine, Phys. Rev. B **26**, 3483 (1982).

[23] J. E. Crowell, J. G. Chen, and J. T. Yates, Surf. Sci. **165**, 37 (1986).

[24] C. Astaldi, P. Geng, and K. Jacobi, J. Electron Spectrosc. Relat. Phenom. **44**, 175 (1987).

[25] C. Engdahl and G. Wahnström, Surf. Sci. **312**, 429 (1994).

[26] G. B. Bachelet, D. R. Hamann, and M. Schlüter, Phys. Rev. B **26**, 4199 (1982).

[27] N. Troullier and J. L. Martins, Phys. Rev. B **43**, 1993 (1991).

[28] M. C. Payne, M. P. Teter, D. C. Allan, T. A. Arias, and J. D. Joannopoulos, Rev. Mod. Phys. **64**, 1045 (1992).

[29] M. J. Gillan, J. Phys. Condens. Matter **1**, 689 (1989)

[30] D. M. Ceperley and B. J. Alder, Phys. Rev. Lett. **45**, 566 (1980); J. P. Perdew and A. Zunger, Phys. Rev. B **23**, 5048 (1981).

[31] J. P. Perdew, J. A. Chevary, S. H. Vosko, K. A. Jackson, M. R. Pederson, D. J. Singh, and C. Fiolhais, Phys. Rev. B **46**, 6671 (1992).

[32] H. B. Nielsen and D. L. Adams, J. Phys. C **15**, 615 (1982).

[33] R. J. Needs, Phys. Rev. Lett. **58**, 53 (1987).

[34] J. Tersoff and D. R. Hamann, Phys. Rev. B **31**, 805 (1985).

[35] C. J. Chen, *Introduction to Scanning Tunneling Microscopy* (Oxford University Press, New York, 1993).

[36] J. Wintterlin, J. Wiechers, H. Brune, T. Gritsch, H. Höfer, and R. J. Behm, Phys. Rev. Lett. **62**, 59 (1989).

[37] A. D. Becke, J. Chem. Phys. **97**, 9173 (1992).

[38] D. A. King, Top. Catalysis **1**, 315 (1994).

[39] F. Besenbacher and J. K. Nørskov, Prog. Surf. Sci. **44**, 5 (1993).

[40] S. A. Flodström, C. W. Martinsson, R. Z. Bachrach, S. B. M. Hagström, and R. S. Bauer, Phys. Rev. Lett. **40**, 907 (1978).

[41] B. Kasemo, E. Törnqvist, J. K. Nørskov, and B. I. Lundqvist, Surf. Sci. **89**, 554 (1979).

[42] L. Hellberg, J. Strömquist, B. Kasemo, and B. I. Lundqvist, Phys. Rev. Lett. **74**, 4742 (1995).

[43] A. Böttcher, R. Imbeck, A. Morgante, and G. Ertl, Phys. Rev. Lett. **65**, 2035 (1994).

[44] K. Hermann, K. Freihube, T. Greber, A. Böttcher, R. Grobecker, D. Fick, and G. Ertl, Surf. Sci. **313**, L806 (1994).

[45] T. Greber, R. Grobecker, A. Morgante, A. Böttcher, and G. Ertl, Phys. Rev. Lett. **70**, 1331 (1993).

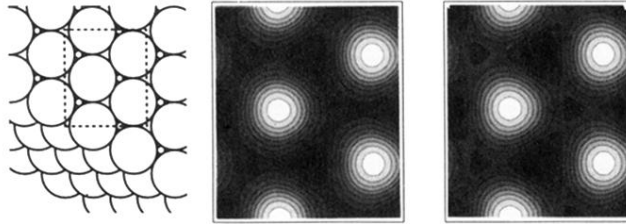[46] A. Böttcher, R. Grobecker, T. Greber, and G. Ertl, Chem. Phys. Lett. **208**, 404 (1993).

FIG. 2. In the middle and to the right, respectively, the calculated contours of constant σ_s (s-type) and σ_{p_z} (p-type) outside a clean Al(111) surface schematically shown to the left. In both cases, the vertical corrugation is 0.15 Å. In the p-type STM the average height above the surface is $\langle z \rangle - z_0 = 0.9$ Å, whereas in the s-type STM $\langle z \rangle - z_0 = 0.1$ Å, z_0 being one Al(111) layer spacing outside the position of the surface layer.
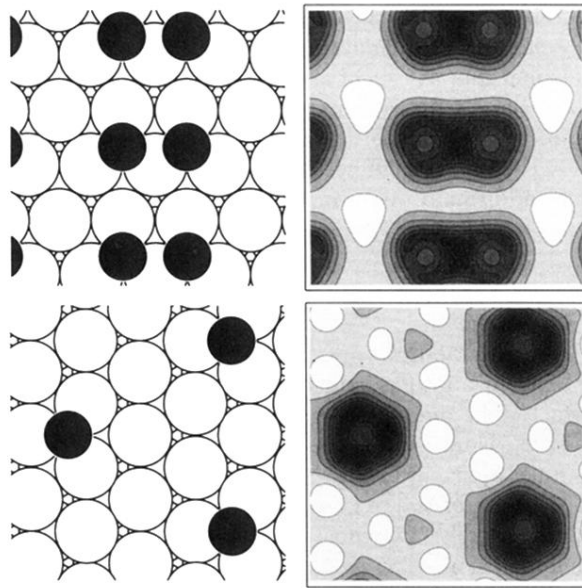
FIG. 8. Above: an oxygen dimer in a $3 \times \sqrt{3}$ unit cell. Below: an oxygen atom in a 3×3 unit cell. To the right calculated STM images are shown, and to the left the atomic positions, with the oxygen atoms small and dark, and the aluminum atoms white. In the STM images, the gray scale is after the height above the surface, in which a local density of states of $0.001\ e(\text{Å}^3\,\text{eV})$ is found. Black is 1.9 Å above the first Al(111) layer, and the spacing is 0.1 Å.